cyclotron for the irradiations; M. McKeown, K. Takahashi, and G. Scharff-Goldhaber for use of the lens spectrometer; M. L. Perlman for use of the $\pi\sqrt{2}$ double focusing spectrometer; A. Sunyar, C. Chasman, and R. A. Ristinen for taking the γ spectrum with their lithium-drifted germanium detector; and J. B. S. Waugh and R. C. Richardson for assistance in the measurement of conversion electrons with a lithium-drifted silicon detector. We are indebted to Dr. K. Takahashi and Dr. M. L. Perlman for valuable discussions, and to Dr. W. Rubinson for reviewing the manuscript.

PHYSICAL REVIEW VOLUME 136, NUMBER 1B 12 OCTOBER 1964

Influence of the Exclusion Principle on the Scattering Theory of Nonlocal, Separable Interactions*

C. B. DUKE†
Palmer Physical Laboratory, Princeton University, Princeton, New Jersey
and
General Electric Research Laboratory, Schenectady, New York

(Received 24 February 1964; revised manuscript received 28 May 1964)

For a nonlocal, separable interaction which describes low-energy nucleon-nucleon scattering, the scattering-theory solution to the Brueckner-Bethe-Goldstone (BBG) equation is obtained analytically. The associated scattering amplitudes are evaluated for all momenta of the interacting pair. The off-energy-shell amplitudes are defined by analytic continuation to complex values of the relative momentum of the pair. The positions of singularities in the amplitudes are investigated for various values of both the two-body kinematical parameters and the density of the passive BBG Fermi gas. A comparison of the amplitudes calculated with and without incorporating the effects of the exclusion principle indicates that even for repulsive interactions the latter may differ from the former by as much as 50% for Fermi-gas densities as low as 1/500 of the observed nuclear density.

A. INTRODUCTION

THE purpose of this paper is the presentation of several results needed in the application of the theory of degenerate many-fermion systems[1] to the computation of the properties of nuclear matter. In particular we wish to treat nuclear matter as a low-density gas of fermions interacting via short-range forces.[2–4] For a perturbation-theory treatment of this system, one needs a solution of the independent-pair[5] two-fermion problem which incorporates the influence of both the exclusion principle and off-energy-shell propagation. In this paper we present such a solution for a case in which it can be obtained analytically.

The new result reported on herein consists of a solution to the Brueckner-Bethe-Goldstone (BBG) equation[6] with scattering theory boundary conditions which is valid for all values of the total momentum of the interacting pair and in which the initial relative momentum of the pair is treated as an arbitrary complex variable. We are able to obtain a solution to the BBG equation in closed form by utilizing a simple two-nucleon interaction, referred to as the WY interaction, introduced independently by Wheeler[7] and Yamaguchi.[8] Yamaguchi discussed the energy-shell scattering theory of this interaction for an isolated pair of nucleons. The energy-shell theory for arbitrary values of the total momentum of the pair was extended to low-density many-fermion systems by Verlet and Gavoret (VG).[9] Numerous more restrictive energy-shell calculations

* This work is based on a portion of a thesis submitted in partial fulfillment of the requirements for a Ph.D. degree at Princeton University, 1963.

† Present address: General Electric Research Laboratory, Schenectady, New York.

[1] See, e.g., J. Goldstone, Proc. Roy. Soc. (London) **A239**, 267 (1957): N. M. Hugenholtz, Physica **23**, 481 (1957); J. Hubbard, Proc. Roy. Soc. (London) **A240**, 539 (1957); V. Galitskii and A. B. Migdal, Zh. Eksperim. i Teor. Fiz. **34**, 139 (1958) [English transl.: Soviet Phys.—JETP **7**, 96 (1958)]; L. D. Landau, Zh. Eksperim. i Teor. Fiz. **30**, 1058 (1956); **32**, 58 (1957); **30**, 97 (1958) [English transl.: Soviet Phys.—JETP **3**, 920 (1957); **5**, 101 (1957); **8**, 70 (1959)]; D. F. Dubois, Ann. Phys. (N. Y.) **7**, 174 (1959); C. B. Duke, Ph.D. thesis, Princeton University, 1963 (unpublished); and A. A. Abrikosov, L. P. Gorkov, and I. E. Dzyaloshinski, *Methods of Quantum Field Theory in Statistical Physics*, translated by R. A. Silverman (Prentice-Hall, Inc., Englewood Cliffs, New Jersey, 1963), Chap. 2.

[2] N. M. Hugenholtz, Physica **23**, 533 (1957).

[3] V. M. Galitskii, Zh. Eksperim. i Teor. Fiz. **34**, 151 (1958) [English transl.: Soviet Phys.—JETP **7**, 104 (1958)]. Prior references embodying similar approaches may be found in this article.

[4] L. Van Hove, Physica **25**, 849 (1959); *Lectures on the Many-Body Problem*, edited by E. R. Caianiello (Academic Press Inc., New York, 1962), p. 5.

[5] L. D. Gomez, J. D. Walecka, and V. F. Weisskopf, Ann. Phys. (N. Y.) **3**, 241 (1958); A. Deshalit and V. F. Weisskopf, *ibid.* **5**, 282 (1958).

[6] H. A. Bethe and J. Goldstone, Proc. Roy. Soc. (London) **A238**, 551 (1957).

[7] J. A. Wheeler, Phys. Rev. **50**, 675 (1936).

[8] Y. Yamaguchi, Phys. Rev. **95**, 1628 (1954).

[9] L. Verlet and J. Gavoret, Nuovo Cimento **10**, 505 (1958).

have been performed using various approximations (e.g., a vanishing total momentum) in order to simplify the computations.[10] Puff has treated the off-energy-shell solutions to a modified scattering problem in the absence of the exclusion principle.[11] In the perturbation-theory treatment of a low-density many-fermion system one needs the analog of Puff's results for a solution to the BBG equation rather than the Schrödinger equation. We have extended the analysis of VG to include the definition and evaluation of the scattering amplitudes for complex values of the initial relative momentum of an interacting pair of fermions. Therefore we are able to determine the influence of the exclusion principle on the location of the pole of the scattering amplitude associated with the bound state of a sufficiently strong interaction. We also investigate the approximation of the independent-pair scattering amplitude by its counterpart for an isolated pair, thereby providing an estimate of the validity of expansions of the former in terms of the latter.[3,10] Although our analysis of the scattering problem is a straightforward generalization of its counterpart for a local potential, the two analyses differ because the WY potential possesses a Born amplitude which is independent of the momentum transfer but dependent on the initial and final relative momenta of the interacting pair. One consequence of this fact is the introduction of an additional double pole in the scattering amplitude for specified purely imaginary values of these relative momenta. The pole disappears when we consider the modified scattering problem needed in a discussion of the dispersion effect in a many-fermion system.[11,12]

The essence of our work is an analysis of the BBG equation for spinless particles:

$$\left[E-\frac{\hbar^2k_1^2}{2m_1}-\frac{\hbar^2k_2^2}{2m_2}-U(\mathbf{k}_1)-U(\mathbf{k}_2)\right]\times\psi_{U,E}(\mathbf{k}_1,\mathbf{k}_2)=\int d^3k_1'd^3k_2'Q(k_F;\mathbf{k}_1,\mathbf{k}_2)\times\langle\mathbf{k}_1,\mathbf{k}_2|V|\mathbf{k}_1',\mathbf{k}_2'\rangle\psi_{U,E}(\mathbf{k}_1',\mathbf{k}_2'), \quad (1)$$

$$Q(k_F;\mathbf{k}_1,\mathbf{k}_2)=\begin{cases}1;\ |\mathbf{k}_1|,\ |\mathbf{k}_2|>k_F\\ 0;\ \text{otherwise.}\end{cases} \quad (2)$$

In Eqs. (1) and (2), $\mathbf{k}_1$ and $\mathbf{k}_2$ denote the wave vectors of the two interacting particles; m_1 and m_2 are their masses; $U(\mathbf{k})$ is the single-particle potential in which they move, $\langle\mathbf{k}_1,\mathbf{k}_2|V|\mathbf{k}_1',\mathbf{k}_2'\rangle$ is the momentum representation of the two-body interaction between them; $Q(k_F;\mathbf{k}_1,\mathbf{k}_2)$ is a projection operator which we are utilizing to incorporate the effect of the exclusion principle; and E is the energy parameter of the two-body system. We have denoted the wave number associated with the Fermi energy by k_F. For spinless particles it is related to the particle density n of the many-fermion system by the expression

$$k_F=(6\pi^2n)^{1/3}. \quad (3)$$

In the spin isotopic-spin formalism,[13] the Fermi wave number is given by

$$k_F=\{6\pi^2n/[(2s+1)(2i+1)]\}^{1/3}, \quad (4)$$

in which s is the spin and i is the isotopic spin of the individual fermions. If the two-body interactions depend only upon scalar combinations of the spin and isotopic spin variables, the calculation of the properties of a low-density system reduces to one which, in effect, involves only spinless particles.

We analyze Eq. (1) because for a low-density system of noninteracting fermions, it describes the scattering of an additional ("incident") fermion, for which $|\mathbf{k}|>k_F$, from one of the fermions in the system. Both the incident particle and those in the original low-density system find themselves in the same single-particle potential $U(\mathbf{k})$. In this communication we will assume that $U(\mathbf{k})=0$. The extension of the analysis to the treatment of $U(\mathbf{k})$ in the effective-mass approximation[12]

$$U(\mathbf{k})\cong U_0+(\hbar^2k^2/2\sigma) \quad (5a)$$

is simple. We replace m by the effective mass

$$m^*\equiv m\sigma/(m+\sigma) \quad (5b)$$

and redefine the zero value of E to lie at $-2U_0$. Our *a priori* selection of $U(\mathbf{k})=0$ implies that the scattering amplitude depends parametrically only on E and k_F in addition to the two-body kinematical parameters. We study the dependence of the scattering amplitude on E for fixed values of k_F.

The applicability of our analysis [or a similar one with $U(\mathbf{k})\neq 0$] for the description of the scattering of a fermion from an actual system of identical fermions is not discussed. Its application to the calculation of the nucleon-nucleus optical potential and the normal-state properties of nuclear matter will be presented in a subsequent communication. The scattering amplitudes associated with the WY interaction are calculated in Sec. B. In Sec. C we present numerical calculations investigating both the detailed structure of the scattering amplitudes and their dependence on the density of the Fermi gas.

[10] See, e.g., K. A. Brueckner and W. Wada, Phys. Rev. **103**, 1008 (1956); C. T. DeDominicis, University of Birmingham, Ph.D. thesis, 1957 (unpublished); C. DeDominicis and P. C. Martin, Phys. Rev. **105**, 1419 (1957); J. Goldstone, Cambridge University, Ph.D. thesis, 1958 (unpublished); M. L. Mehta, Nucl. Phys. **12**, 333 (1959); J. S. R. Chisholm and E. J. Squires, *ibid.* **13**, 165 (1959); P. C. Sood and S. A. Moszkowski, *ibid.* **21**, 582 (1960); and J. Dabrowski and J. Sawicki, *ibid.* **22**, 318 (1961).

[11] R. D. Puff, Ann. Phys. (N. Y.) **13**, 317 (1961).

[12] K. A. Brueckner and W. Wada, Phys. Rev. **103**, 1008 (1956).

[13] See, e.g., J. M. Blatt and V. F. Weisskopf, *Theoretical Nuclear Physics* (John Wiley & Sons, Inc., New York, 1952), p. 153.

B. CALCULATION OF THE INDEPENDENT-PAIR SCATTERING AMPLITUDES

We analyze Eq. (1) for the case in which $U(\mathbf{k})=0$ and the two-body interaction term is a linear transformation of rank one. Introducing the definitions:

$$\mathbf{\Lambda}\equiv\mathbf{k}_1+\mathbf{k}_2; \qquad \Lambda=|\mathbf{\Lambda}|, \tag{6a}$$

$$\mathbf{k}\equiv\mu\left(\frac{\mathbf{k}_1}{m_1}-\frac{\mathbf{k}_2}{m_2}\right); \quad k=|\mathbf{k}|, \tag{6b}$$

$$\mu\equiv m_1m_2/(m_1+m_2), \tag{6c}$$

we write the interaction as

$$\langle\mathbf{k}_1,\mathbf{k}_2|\,V\,|\mathbf{k}_1',\mathbf{k}_2'\rangle=\delta(\mathbf{\Lambda}-\mathbf{\Lambda}')\langle\mathbf{k}|\,V\,|\mathbf{k}'\rangle, \tag{7a}$$

$$\langle\mathbf{k}|\,V\,|\mathbf{k}'\rangle=-\lambda g_0(k)g_0(k'). \tag{7b}$$

The subscript zero on $g_0(k)$ indicates that the interaction causes only isotropic scattering, and the symbol $\delta(x)$ denotes the Dirac delta function.[14] The interaction (7) is written in accordance with the assumed invariance of the two-body system under rotations, reflections, time reversal, and Galilean transformations. It can be shown[15] that the scattering amplitude resulting from the solution to (1) for the interaction (7) is given by

$$f_{\Lambda_0}(\mathbf{k},\mathbf{k}_0)=\frac{4\pi^2\lambda\mu}{\hbar^2}\times\frac{[g_0(k_0)]^2}{1-\chi(k_F;\,k_0,\Lambda_0)}, \tag{8}$$

$$\chi(k_F;\,k_0,\Lambda_0)=\frac{2\mu\lambda}{\hbar^2}\int_0^\infty\frac{[g_0(k)]^2Q(k_F;\,k,\Lambda_0)k^2dk}{k^2-k_0^2-i\epsilon}, \tag{9}$$

in which $\mathbf{\Lambda}_0$ denotes the initial total momentum of the interacting pair and $\mathbf{k}_0$ denotes the initial relative momentum. The limit $\epsilon\to 0^+$ is understood in Eq. (9) and the projection operator $Q(k_F;\,k,\Lambda_0)$ is obtained from Figs. 1 and 2 for $\Lambda_0>2k_F$ and $\Lambda_0<2k_F$, respectively. We find:

Case I: $\Lambda_0>2k_F$

$$Q(k_F;k,\Lambda_0)=4\pi; \quad k<[(\Lambda_0/2)-k_F] \quad \text{or} \quad k>[(\Lambda_0/2)+k_F], \tag{10a}$$

$$Q(k_F;k,\Lambda_0)=4\pi\left[\frac{k^2+(\Lambda_0/2)^2-k_F^2}{k\Lambda_0}\right]; \quad [(\Lambda_0/2)-k_F]\leq k\leq[(\Lambda_0/2)+k_F]. \tag{10b}$$

Case II: $\Lambda_0<2k_F$

$$Q(k_F;k,\Lambda_0)=0; \quad k<[k_F^2-(\Lambda_0/2)^2]^{1/2}, \tag{11a}$$

$$Q(k_F;k,\Lambda_0)=4\pi\left[\frac{k^2+(\Lambda_0/2)^2-k_F^2}{k\Lambda_0}\right]; \quad [k_F^2-(\Lambda_0/2)^2]^{1/2}\leq k\leq[(\Lambda_0/2)+k_F], \tag{11b}$$

$$Q(k_F;k,\Lambda_0)=4\pi; \quad k>[(\Lambda_0/2)+k_F]. \tag{11c}$$

The analysis can readily be extended to arbitrary interactions of finite rank, although, in general, the projection operators depend on the direction as well as the magnitude of $\mathbf{\Lambda}_0$.[15,16]

The relationship between the energy conserving matrix elements of the two-fermion T matrix[17] and the

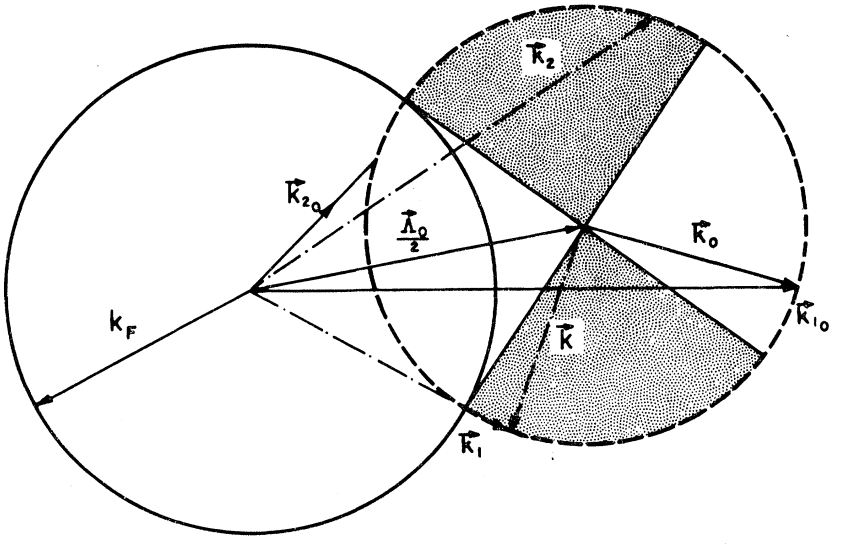

FIG. 1. A schematic illustration of the exclusion-principle restrictions on the kinematics when one-half the center-of-mass wave vector terminates outside the Fermi sphere. The solid circle indicates the Fermi sphere and the dashed circle the energy-momentum shell. The shaded area delineates those angles between the final relative wave vector $\mathbf{k}$, and the center-of-mass wave vector $\mathbf{\Lambda}_0$, which are permitted by the exclusion-principle restrictions. The figure is rotationally symmetric about an axis through $\mathbf{\Lambda}_0$.

[14] P. A. M. Dirac, *The Principles of Quantum Mechanics* (The Clarendon Press, Oxford, 1958), p. 58.
[15] C. B. Duke, General Electric Research Laboratory Report 64-RL-(3604M) (unpublished).
[16] R. Courant and D. Hilbert, *Methods of Mathematical Physics* (Interscience Publishers, Inc., New York, 1955), Vol. I, Chap. 3.
[17] See, e.g., L. H. Schick, Rev. Mod. Phys. **33**, 608 (1961).

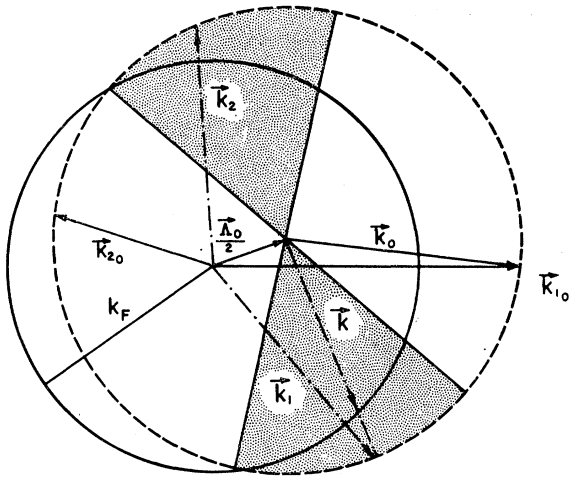

FIG. 2. A schematic illustration of the exclusion-principle restrictions on the kinematics when one-half the center-of-mass wave vector terminates within the Fermi sphere. The solid circle indicates the Fermi sphere and the dashed circle the energy-momentum shell. The shaded area delineates those angles between the final relative wave vector $\mathbf{k}$ and the center-of-mass wave vector $\mathbf{\Lambda}_0$, which are permitted by the exclusion-principle restrictions. The figure is rotationally symmetric about an axis through $\mathbf{\Lambda}_0$.

scattering amplitude is given by[15]

$$\langle \mathbf{k}(k_0/k)\,|\,T_{\Lambda_0}|\,\mathbf{k}_0\rangle = -(\hbar^2/4\pi^2\mu) f_{\Lambda_0}(\mathbf{k},\mathbf{k}_0). \quad (12)$$

We confine our attention to the calculation of the scattering amplitudes $f_{\Lambda_0}(\mathbf{k},\mathbf{k}_0)$. By permitting k_0 to be an arbitrary complex variable we obtain via (12) matrix elements of the T matrix related to those needed to discuss the dispersion effect in a low-density many-fermion system. The general T-matrix elements are given by

$$\langle \mathbf{k}'\,|\,T_{\Lambda_0}[\hbar^2 k_0^2/2\mu + \hbar^2\Lambda_0^2/2(m_1+m_2)]\,|\,\mathbf{k}\rangle = -\frac{\lambda g_0(k') g_0(k)}{1-\chi(k_F; k_0,\Lambda_0)}. \quad (13)$$

If $k' \neq k$ and k', k, and k_0 are arbitrary complex variables, then Eq. (13) specifies the general "off-energy-shell" matrix elements. The particular matrix element needed in a discussion of the dispersion effect[3,11,12] is that obtained from (13) when both k' and k are equal to each other and are on the energy shell while χ is computed for arbitrary complex values of k_0.

In order to extend the results of Verlet and Gavoret[9] we analyze the Wheeler-Yamaguchi potential[7,8] which is specified by

$$g_0(k) = \left[\frac{2\pi\hbar^2}{\mu}\right]^{1/2} \frac{1}{k^2+\beta^2}. \quad (14)$$

Using Eqs. (9), (10), and (11) we compute $\chi(k_F; k_0,\Lambda_0)$ in a straightforward manner. The results can be expressed compactly by writing $\chi(k_F;k_0,\Lambda_0)$ as the boundary value of a function of the complex variable z, i.e., $\chi(k_F; z,\Lambda_0)$, such that

$$\chi(k_F;k_0,\Lambda_0) = \begin{cases} \lim_{\epsilon\to 0^+} \chi(k_F;k_0+i\epsilon,\Lambda_0); & k_0^2>0 \\ \lim_{\epsilon\to 0^+} \chi(k_F;\epsilon+i|k_0|,\Lambda_0); & k_0^2<0. \end{cases} \quad (15)$$

The appropriate functions $\chi(k_F; z,\Lambda_0)$ for the two cases specified by Eqs. (10) and (11) are

Case I: $(\Lambda_0/2) \geq k_F$

$$\chi(k_F,z,\Lambda_0) = \frac{2\pi\lambda}{(\beta^2+z^2)^2}\left\{\frac{\beta^2-z^2}{\beta}\left[\frac{\pi}{2} - \tan^{-1}\left(\frac{2k_F\beta}{(\Lambda_0/2)^2+\beta^2-k_F^2}\right)\right] + \frac{(\Lambda_0/2)^2+z^2-k_F^2}{\Lambda_0} \times \ln\left[\frac{[z^2-(\Lambda_0/2+k_F)^2][\beta^2+(\Lambda_0/2-k_F)^2]}{[z^2-(\Lambda_0/2-k_F)^2][\beta^2+(\Lambda_0/2+k_F)^2]}\right] + z\ln\left[\frac{(z+\Lambda_0/2+k_F)(z-\Lambda_0/2+k_F)}{(z+\Lambda_0/2-k_F)(\Lambda_0/2+k_F-z)}\right]\right\}. \quad (16a)$$

Case II:

$$\chi(k_F; z,\Lambda_0) = \frac{2\pi\lambda}{(\beta^2+z^2)^2}\left\{\frac{\beta^2-z^2}{\beta}\left[\frac{\pi}{2} - \tan^{-1}\left(\frac{\Lambda_0/2+k_F}{\beta}\right)\right] + \frac{(\Lambda_0/2)^2+z^2-k_F^2}{\Lambda_0} \times \ln\left[\frac{[z^2-(\Lambda_0/2+k_F)^2][\beta^2+k_F^2-(\Lambda_0/2)^2]}{[(\Lambda_0/2)^2-k_F^2+z^2][(\Lambda_0/2+k_F)^2+\beta^2]}\right] + z\ln\left[\frac{\Lambda_0/2+k_F+z}{\Lambda_0/2+k_F-z}\right]\right\}. \quad (16b)$$

The analytic structure of $\chi(k_F; k_0,\Lambda_0)$ is illustrated in Fig. 3. The solid and wavy lines along the real k_0 axis indicate logarithmic branch cuts. Only the cut indicated by the wavy line would be present if we restricted the parameter E to the energy shell. At the branch points terminating these cuts, the slope of the imaginary part of $\chi(k_F; k_0,\Lambda_0)$ undergoes a discontinuous change and the slope of the real part of $\chi(k_F; k_0,\Lambda_0)$ becomes either positively or negatively infinite. The former effect can cause the appearance of cusp-like structures in the scattering amplitude. The latter effect influences the structure of the scattering amplitudes very little.

We assign to all the particles inside the Fermi sphere the free-particle energy-momentum relation. The energy of the incident fermion outside the Fermi sphere is used as the independent energy variable. This energy variable is related to a wave number s_0 via

$$E_1 \equiv \hbar^2 s_0^2/2m_1. \tag{17}$$

If $s_0=k_{1_0}$, the two-body scattering occurs "on the energy shell." In general, the complex variable k_0 is defined by

$$k_0^2 \equiv [(k_{2_0}^2+s_0^2)/2]-(\Lambda_0/2)^2, \tag{18a}$$

$$k_0 \equiv \begin{cases} [k_0^2]^{1/2}; & k_0^2 \geq 0 \\ i[|k_0^2|]^{1/2}; & k_0^2 < 0 \end{cases}. \tag{18b}$$

We set $m_1=m_2$ and put them both equal to the nucleon mass in Eqs. (1) and (6).

The scattering amplitude for the Wheeler-Yamaguchi (WY) potential is specified by Eqs. (8), (14), and (16). In the $k_F \to 0$ limit, expression (8) reduces to the one given by Yamaguchi.[8] Equation (1) fails to have a scattering solution if and only if the equation

$$\chi(k_F; k_0, \Lambda_0)=1 \tag{19}$$

has a solution.[16] When (19) is satisfied, the scattering amplitude has a singularity which signals the failure of the scattering boundary-value problem to have a solution. Due to the complicated structure of Eqs. (16), we investigate the existence of solutions to (19) numerically. However, it is easy to verify that the scattering amplitude has a "spurious" pole at

$$k_0=i\beta \tag{20a}$$

for all values of Λ_0.

In the absence of the exclusion principle both the scattering amplitude and the collision matrix exhibit a double pole at k_0 given by (20a) and (for $k_0 \neq \pm i\beta$) simple poles at

$$k_0=-i[\beta+\pi(\lambda/\beta)^{1/2}], \tag{20b}$$

$$k_0=-i[\beta-\pi(\lambda/\beta)^{1/2}]. \tag{20c}$$

If $\lambda > \beta^3/\pi^2$ the pole whose location is given by (20c) corresponds to a bound state. Yamaguchi[8] has given the wave function of both the bound state and the continuum state. One can easily verify that the bound-state wave function is orthogonal to the continuum wave function even for complex values of k_0. The double pole whose location is given by (20a) results from the failure of the scattering problem to have a solution if $k_0=i\beta$. It does not correspond directly to the "redundant" poles occurring in the scattering theory of local potentials at which values of k_0 the scattering-theory solution to (1) is identically zero. If $\mathrm{Im}(k_0)>\beta$, the contribution to the outgoing wave from the poles of the WY interaction is larger than the contribution from the analytic continuation of the physical scattered wave.

TABLE I. The parameters of the Wheeler-Yamaguchi (Refs. 7 and 8) potential which reproduces with the low-energy neutron-proton effective range data.[a] The potential is specified by Eqs. (7) and (14) in the text.

Spin (S)	Isotopic spin (I)	λ (F^{-3})	β (F^{-1})
0	1	0.154	1.180
1	0	0.425	1.460

[a] M. H. MacGregor, M. J. Moravsick, and H. P. Stapp. Ann. Rev. Nucl. Sci. 10, 291 (1960).

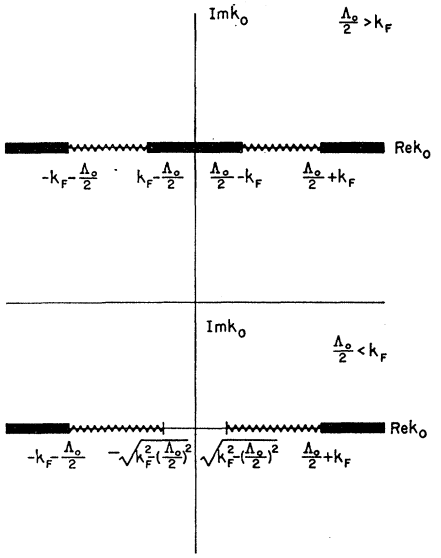

FIG. 3. A schematic illustration of the analytic struction of $\chi(k_F; k_0, \Lambda_0)$ given by Eqs. (15) and (16) in the text. The center-of-mass wave vector $\mathbf{\Lambda}_0$ is fixed so that the analytic structure is given by considering $\chi(k_F; k_0, \Lambda_0)$ to be a function of k_0 alone. Both the solid and wavy lines indicate logarithmic cuts.

C. NUMERICAL CALCULATIONS

Our model of two-body scattering in a low-density many-fermion system utilizes five parameters, λ, β, $|\mathbf{k}|$, $|\mathbf{\Lambda}|$, and k_F to describe a particular scattering. For each combination of these five parameters we analyze the two-body scattering of an incident particle above the Fermi sphere from a particle below the Fermi sphere as a function of the (independent) energy variable s_0 defined by Eq. (17). We require that $s_0 \geq k_F$. The influence of the sign and magnitude of the potential on the scattering was investigated by performing the analyses described below for four potentials: the singlet and triplet nucleon-nucleon potentials specified in Table I, and their repulsive counterparts. Because of the role which low-density expansions have played in previous analyses,[3,4] we first investigate the influence of the parameter k_F on the scattering amplitudes resulting from the above potentials. We then examine the scattering of a single nucleon from a noninteracting Fermi gas of the observed nuclear density.

As the interaction specified by Eq. (7b) causes scat-

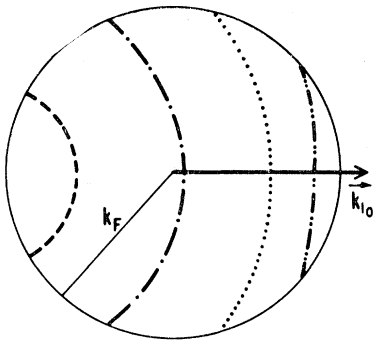

FIG. 4. A schematic illustration of sets of particles within the Fermi sphere which, when paired with an incident particle having the wave vector $\mathbf{k}_{10}$, lead to center-of-mass wave vectors $\mathbf{\Lambda}_0$ of equal magnitude. The solid circle indicates the Fermi sphere. The dashed, dot-dashed, dotted, and dashed-double-dotted arcs are loci of the terminating points of wave vectors which lead to a fixed value of Λ_0. The value of Λ_0 associated with these arcs increases monotonically as one moves from the dashed arc to the dashed-double-dotted arc.

tering only in states with angular momentum zero, the scattering amplitude depends only on the magnitude of $\mathbf{\Lambda}_0$. We see from Fig. 4 that for a given value of $\mathbf{k}_{10}$ the wave vectors of the Fermi-gas particles which yield the same value of the center-of-mass wave number Λ_0 lie on arcs of circles of radius Λ_0. The scattering amplitudes associated with the incident particle plus each of the particles whose wave vectors terminate on a particular arc are given by (8) for the appropriate (fixed) value of Λ_0. For a given value of Λ_0, the smallest value of k_0^2 in (8) is associated with the Fermi-gas particle whose wave vector lies parallel (or antiparallel) to that

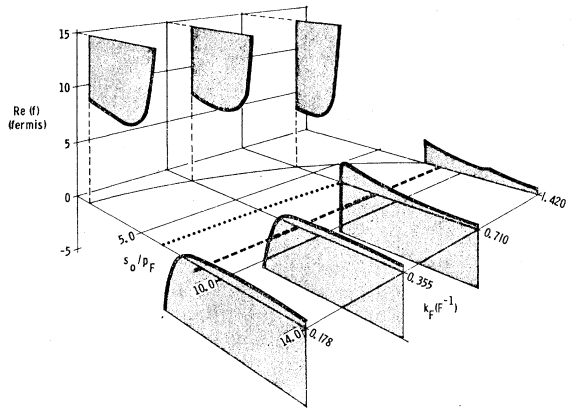

FIG. 5. The real part of the independent-pair scattering amplitude calculated for the Wheeler-Yamaguchi potential (Refs. 7, 8) with the parameters $\lambda=0.425$ F^{-3} and $\beta=1.46$ F^{-1}. The calculations were performed using Eqs. (8), (15), and (16) in the text with the kinematical parameters $k_{10}=1.562$ F^{-1}, $k_{20}=0.1775$ F^{-1}, and $\cos\theta=1.0$. The solid lines represent the real part of the scattering amplitude. The shading is included only for ease in visualization. The heavy dashed line indicates the energy-shell value, k_{10}, of s_0. The dotted line designates the location of the bound-state pole in the scattering amplitude. The curving light line at which the graphs of Re(f) begin indicates the point $s_0=k_F$ for the various values of k_F. The s_0 scale is measured in units of $p_F=(k_F)_{\text{obs}}/8$.

of the incident fermion. The graphs of the scattering amplitude versus k_0^2 associated with other Fermi-gas particles which yield the same value of Λ_0 may be obtained from the graph associated with the parallel-wave-vector particle by (a) starting the scale at the appropriate (larger) value of k_0^2, and (b) expanding the k_0^2 scale. Therefore, for the WY potential we discuss only the scattering amplitudes associated with parallel-wave-vector Fermi-gas particles. We present in the figures results obtained from the nucleon-nucleon spin-triplet potential. This potential has a bound state in the absence of exclusion-principle effects. The shift in the location of (or suppression of) the pole in the scattering amplitude associated with this bound state provides one of the most graphic examples of the effects of the exclusion principle on the two-body scattering problem.

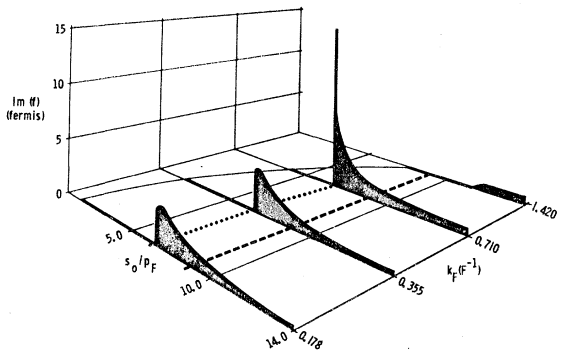

FIG. 6. The imaginary part of the independent-pair scattering amplitude calculated for the Wheeler-Yamaguchi (Refs. 7, 8) potential with the parameters $\lambda=0.425$ F^{-3} and $\beta=1.46$ F^{-1}. The calculations were performed using Eq. (8), (15), and (16) in the text with the kinematical parameters $k_{10}=1.562$ F^{-1}, $k_{20}=0.1775$ F^{-1}, and $\cos\theta=1.0$. The solid lines represent the imaginary part of the scattering amplitude. The shading is included only for ease in visualization. The heavy dashed line indicates the energy-shell value, k_{10}, of s_0. The dotted line designates the location of the bound-state pole in the scattering amplitude. The curving light line at which the graphs of Im(f) begin indicates the point $s_0=k_F$ for the various values of k_F. The s_0 scale is measured in units of $p_F=(k_F)_{\text{obs}}/8$.

For a given potential, the dependence of the scattering amplitude on the density of the Fermi gas (i.e., on k_F) is investigated in two ways. In the first method, to which we refer as the method of absolute kinematics, we fix the wave vectors of the two scattering particles subject to the constraint that for all values of k_F investigated one vector lies outside and one inside the Fermi sphere. In Figs. 5–8 we show the real and imaginary parts of the scattering amplitudes associated with the scattering, via the spin-triplet potential, of an incident particle, from two particles in the Fermi gas. The wave vector of the incident particle has a magnitude $k_{10}=1.562$ F^{-1} while those of the two Fermi-gas particles have a magnitude $p_F=(k_F)_{\text{obs}}/8$ and are oriented parallel and antiparallel to the wave vector of the incident particle. The "observed" Fermi wave number, $(k_F)_{\text{obs}}$, is obtained

from fast-electron scattering data.[18] It is given by

$$(k_F)_{\text{obs}}=1.42\ \text{F}^{-1}. \tag{21}$$

An outstanding feature of Figs. 5 and 7 is their illustration of the movement of the bound-state pole toward zero energy as k_F increases. The strong suppression of the scattering of the incident particle from a particle far inside the Fermi sphere is also evident from the figures. We note, however, that this suppression is by no means monotonic with increasing k_F. When the bound-state pole lies close to zero energy (of the pair), the imaginary part of the scattering amplitude is greatly enhanced over its isolated-pair value.

As opposed to the spin-triplet results illustrated in Figs. 5 and 7, the real part of the scattering amplitude

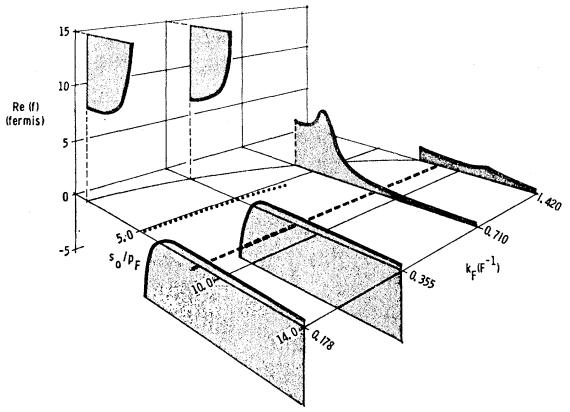

FIG. 7. The real part of the independent-pair scattinerg amplitude calculated for the Wheeler-Yamaguchi (Refs. 7, 8) potential with the parameters $\lambda=0.425\ \text{F}^{-3}$ and $\beta=1.46\ \text{F}^{-1}$. The calculations were performed using Eqs. (8), (15), and (16) in the text with the kinematical parameters $k_{1_0}=1.562\ \text{F}^{-1}$, $k_{2_0}=0.1775\ \text{F}^{-1}$, and $\cos\theta=-1.0$. The solid lines represent the real part of the scattering amplitude. The shading is included only for ease in visualization. The heavy dashed line indicates the energy-shell value, k_{1_0}, of s_0. The dotted line designates the location of the bound-state pole in the scattering amplitude. The curving light line at which the graphs of $\text{Re}(f)$ begin indicates the point $s_0=k_F$ for the various values of k_F. The s_0 scale is measured in units of $p_F=(k_F)_{\text{obs}}/8$.

for the spin-singlet potential remains positive everywhere. However, when $(\Lambda_0/2)>k_F$, the real part of the scattering amplitude can develop a sharp spike near $k_0=0$ because of the large low-energy nucleon-nucleon cross sections associated with the singlet potential. At small values of Λ_0, the singlet scattering amplitude is depressed by a factor of 2 relative to the triplet amplitude. This depression almost vanishes for $\Lambda_0\gtrsim 1.0k_F$.

Repulsive potentials give a real part of the scattering amplitude which is everywhere negative (corresponding to a positive zero-energy scattering length[19]). The magnitude of both the real and imaginary parts of the

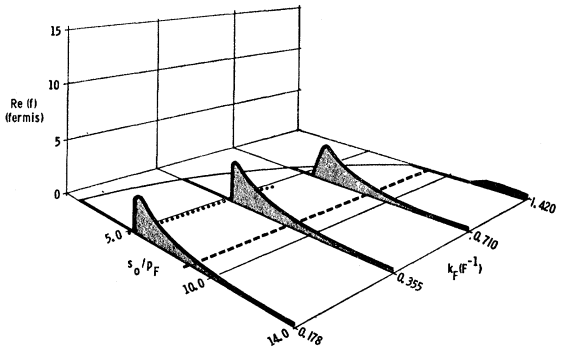

FIG. 8. The imaginary part of the independent-pair scattering amplitude calculated for the Wheeler-Yamaguchi (Refs. 7, 8) potential with the parameters $\lambda=0.425\text{F}^{-3}$ and $\beta=1.46\ \text{F}^{-1}$. The calculations were performed using Eqs. (8), (15), and (16) in the text with the kinematical parameters $k_{1_0}=1.562\ \text{F}^{-1}$, $k_{2_0}=0.1775\ \text{F}^{-1}$, and $\cos\theta=-1.0$. The solid lines represent the imaginary part of the scattering amplitude. The shading is included only for ease in visualization. The heavy dashed line indicates the energy-shell value, k_{1_0}, of s_0. The dotted line designates the location of the bound-state pole in the scattering amplitude. The curving light line at which the graphs of $\text{Im}(f)$ begin indicates the point $s_0=k_F$ for the various values of k_F. The s_0 scale is measured in units of $p_F=(k_F)_{\text{obs}}/8$.

scattering amplitude is characteristically about an order of magnitude below that obtained for attractive potentials of the same strength and range. Using the method of absolute kinematics with the parameters used in Figs. 5–8, we find that for $k_F=(k_F)_{\text{obs}}/8$ the scattering amplitudes obtained with and without the exclusion principle are identical to within 1%. At the observed nuclear density, however, the imaginary part of the scattering amplitude calculated with the exclusion principle is below that calculated without the exclusion principle by a factor of two or more until k_0^2 greatly exceeds its energy-shell value. The real part of the scattering amplitude is quite close to the isolated-pair value for $k_0/\beta>1.0$, although for the lower of k_0/β permitted values by the exclusion principle its values can be as much as a factor of 1.8 below the isolated-pair value. (For example, this occurs at $k_0/\beta=0.350$ using the repulsive spin-triplet potential.) The deviation of the scattering amplitudes from their isolated-pair values is much less severe at $k_F=(k_F)_{\text{obs}}/2$. For this value of k_F the maximum deviation (for the kinematics corresponding to those used in Figs. 5–8) is of the order of 20% of the isolated-pair value.

In the second method of investigating the dependence of the scattering amplitude on the density we fix the ratios (k_{1_0}/k_F) and (k_{2_0}/k_F) during the variations of k_F. We refer to this procedure as the method of relative kinematics because the ratio k_{1_0}/k_{2_0} is constant although the magnitudes k_{1_0} and k_{2_0} vary with k_F. This method permits us to investigate the effect of the exclusion principle on low-energy scatterings in a low-density gas. The scattering amplitudes for the spin-triplet potential are illustrated in Figs. 9–12. In the method of relative kinematics, each set of values (k_{1_0},k_{2_0}) is associated with

[18] D. G. Ravenhall, Rev. Mod. Phys. **30**, 430 (1958).

[19] See, e.g., H. A. Bethe and P. Morrison, *Elementary Nuclear Theory* (John Wiley & Sons, Inc., New York, 1956), 2nd ed., Chap. 10.

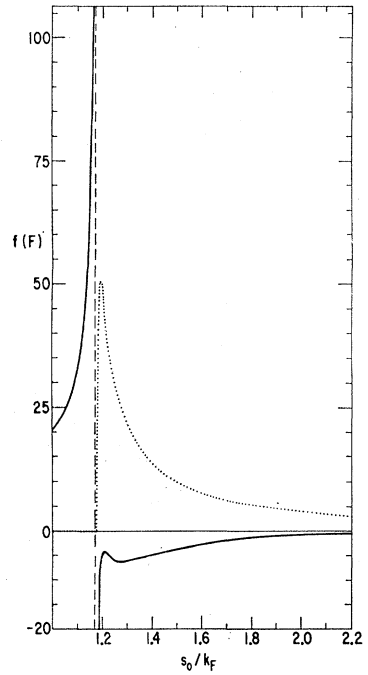

FIG. 9. Real and imaginary parts of an independent-pair scattering amplitude calculated for the Wheeler-Yamaguchi (Refs. 7, 8) potential with the parameters $\lambda=0.425$ F^{-3}, $\beta=1.46$ F^{-1} and $k_F=0.355$ F^{-1}. The calculations were performed using Eqs. (8), (15), and (16) in the text. The solid and dotted lines represent the real and imaginary parts, respectively, of the scattering amplitude obtained for $(k_{10}/k_F)=1.2$, $(k_{20}/k_F)=0.9$ and $\cos\theta=1.0$.

a different value of Λ_0. The vanishing of the energy-shell values of the imaginary part of the scattering amplitude, Im(f), for the $k_{2_0}=0.7\ k_F$ curves in Figs. 9–12 illustrates exclusion-principle suppression even at low densities of the energy-shell scattering from fermions inside the Fermi sphere. This effect is large only if the wave vector which terminates outside the Fermi sphere lies near the Fermi sphere. When $k_{2_0}=1.6\ k_F$ the effect has disappeared entirely. Figures 9–12 as well as Figs. 5–8 illustrate the suppression of the bound-state pole for large values of k_F. The solid curve in Fig. 10 shows the real part of the scattering amplitude which results when the pole moves to complex values of k_0^2. We also find poles at positive values of k_0^2 corresponding to the "positive-energy bound states" (Cooper states) in the theory of nuclear matter.[20] The dotted curves in Figs. 9 and 10 illustrate again the great enhancement of the imaginary part of the scattering amplitude, both on and off the energy shell, which results when the bound-state pole approaches $k_0^2=0$. The energy-shell value of Im(f) associated with Fig. 9 is larger by a factor of 30 than its isolated value. We conclude that for low-energy scattering, the approximation of the scattering amplitude by its isolated-pair value is nowhere valid within our range of values for k_F: $[(k_F)_{\rm obs}/8]\leq k_F\leq(k_F)_{\rm obs}$.

[20] See, e.g., R. L. Becker, Phys. Rev. 127, 1328 (1962).

The effects of the exclusion principle on the repulsive counterpart of the nucleon-nucleon spin-triplet potential are less noticeable than those illustrated in Figs. 9–12. However, using the method of relative kinematics with the same parameters as those employed in Figs. 9–12, we find that for $k_F=(k_F)_{\rm obs}/8$ the imaginary part of the scattering amplitude can be suppressed by a factor of 2 from its isolated-pair value. In addition, the small cusp-like structures in Re(f) which were discussed in the last section are readily discernable at the appropriate values of k_0. The suppression of the values of Im(f) by a factor of about 2 persists at higher densities. In addition, when $k_F=(k_F)_{\rm obs}/2$ the real part of the scattering amplitude lies below its isolated-pair value by as much as 20% of the isolated-pair value. This result occurs also for the kinematics associated with Figs. 5–8. We conclude that even for a *repulsive* triplet potential the imaginary part of the scattering amplitude for low-energy scatterings is never satisfactorily approximated by the isolated-pair value. Such an approximation for the real part of the scattering amplitude is less accurate than 20% for values of k_F above one-half $(k_F)_{\rm obs}$. For all values of k_F, the approximation is more satisfactory for high-energy than for low-energy scatterings.

The scattering of an incident fermion from those in a Fermi gas with $k_F=(k_F)_{\rm obs}$ was investigated in detail

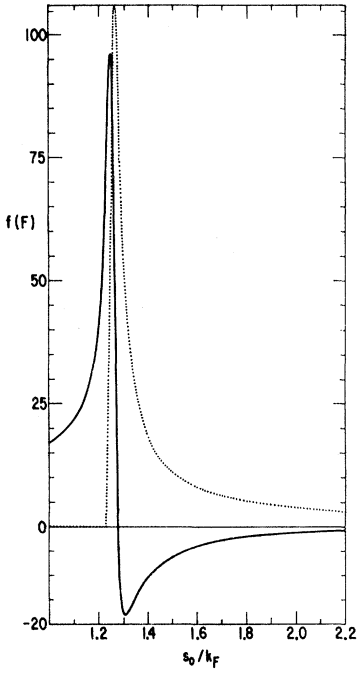

FIG. 10. Real and imaginary parts of an independent-pair scattering amplitude calculated for the Wheeler-Yamaguchi (Refs. 7, 8) potential with the parameters $\lambda=0.425$ F^{-3}, $\beta=1.46$ F^{-1}, and $k_F=0.355$ F^{-1}. The calculations were performed using Eqs. (8), (15), and (16) in the text. The solid and dotted lines represent the real and imaginary parts, respectively, of the scattering amplitude obtained for $(k_{10}/k_F)=1.2$, $(k_{20}/k_F)=0.7$ and $\cos\theta=1.0$.

for both the spin-singlet and spin-triplet potentials with $k_{1_0}=1.2\ k_F$, $1.6\ k_F$, and $2.0\ k_F$. Using Eqs. (18) for k_0^2 and the expression

$$\Lambda_0^2=k_{1_0}^2+k_{2_0}^2+2k_{1_0}k_{2_0}\cos\theta\,, \tag{22a}$$

$$\theta\equiv\theta_{k_{10},k_{2_0}}\,, \tag{22b}$$

for Λ_0, we calculated the scattering amplitudes for a grid in which $k_{1_0}=0.0, 0.1\ k_F, \cdots, 1.0\ k_F$ and $\cos\theta=-1.0$, 0.0, and 1.0. These calculations, as well as those presented above, were performed on the GE 225 computer at the General Electric Research Laboratory.

We first discuss the spin-triplet potential specified by Table I and Eqs. (7) and (14). For $s_0=k_F$, we find from (18) and (22) that none of the particles in the Fermi gas gives rise to a nonzero value of Im(f). If $(\Lambda_0/2)>k_F$ then $k_0^2<0$. Therefore, the scattering "occurs" sufficiently far below the energy shell that Im(f)=0. If $(\Lambda_0/2)\leq k_F$ then the exclusion principle requires that Im(f)=0. Letting s_0 become greater than k_F, we find that for $\Lambda_0<2.3\ k_F$ the bound-state pole in the scattering amplitude is suppressed by the exclusion principle. However, for $2.0\ k_F\leq\Lambda_0\leq 2.3\ k_F$, the scattering amplitudes exhibit sharp structure near $k_0=0$ as illustrated in Fig. 12. When $k_{1_0}=1.2\ k_F$, the maximum value of Λ_0 is $2.2\ k_F$ so that the bound-state pole does not appear. It appears for $k_{2_0}\geq 0.8\ k_F$ when $k_{1_0}=1.6\ k_F$ and for $k_{2_0}\geq 0.4\ k_F$ when $k_{1_0}=2.0\ k_F$. In the latter case, we also see the spurious pole characteristic of the WY potential when $s_0<1.4\ k_F$.

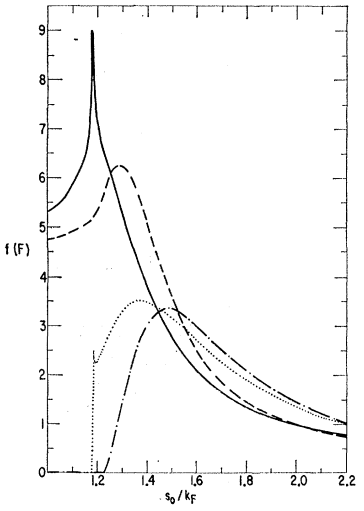

FIG. 11. Real and imaginary parts of independent-pair scattering amplitudes calculated for the Wheeler-Yamaguchi (Refs. 7, 8) potential with the parameters $\lambda=0.425$ F^{-3}, $\beta=1.46$ F^{-1}, and $k_F=0.710$ F^{-1}. The calculations were performed using Eqs. (8), (15), and (16) in the text. The solid and dotted lines represent the real and imaginary parts, respectively, of the scattering amplitude obtained for $(k_{10}/k_F)=1.2$, $(k_{20}/k_F)=0.9$, and $\cos\theta=1.0$. The dashed and dot-dashed lines show the real and imaginary parts, respectively, of the scattering amplitude obtained for $(k_{10}/k_F)=1.2$, $(k_{20}/k_F)=0.7$, and $\cos\theta=1.0$.

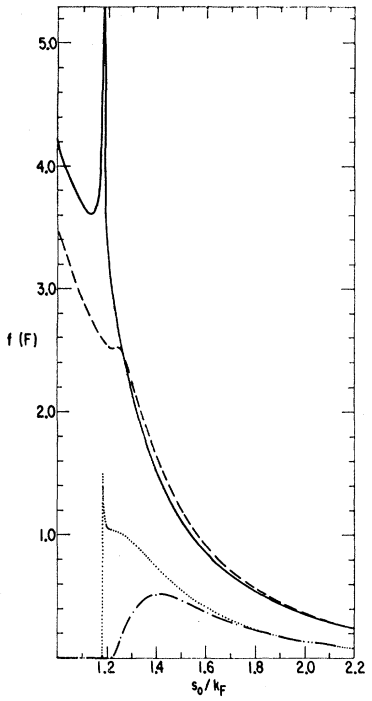

FIG. 12. Real and imaginary parts of independent-pair scattering amplitudes calculated for the Wheeler-Yamaguchi (Refs. 7, 8) potential with the parameters $\lambda=0.425$ F^{-3}, $\beta=1.46$ F^{-1}, and $k_F=1.42$ F^{-1}. The calculations were performed using Eqs. (8), (15), and (16) in the text. The solid and dotted lines represent the real and imaginary parts, respectively, of the scattering amplitude obtained for $(k_{10}/k_F)=1.2$, $(k_{20}/k_F)=0.9$, and $\cos\theta=1.0$. The dashed and dot-dashed lines show the real and imaginary parts, respectively, of the scattering amplitude obtained for $(k_{10}/k_F)=1.2$, $(k_{20}/k_F)=0.7$, and $\cos\theta=1.0$.

When the value of s_0 is close to k_F, only those Fermi-gas particles for which $k_{2_0}\cong k_F$ and $\cos\theta\cong-1$ give rise to nonzero Im(f). However, as s_0 increases, particles with smaller values of k_{2_0} and larger values of $\cos\theta$ begin to contribute positive values of Im(f). For $k_{1_0}=1.2\ k_F$, no particles with $k_{2_0}\leq 0.7\ k_F$ yield nonzero energy-shell Im(f). At that value of s_0 at which Im(f) becomes nonzero, the real part of the scattering amplitude exhibits a characteristic rise the magnitude of which diminishes with increasing values of Λ_0 until $\Lambda_0=2.0\ k_F$. This effect is illustrated in Fig. 13. Although the figure shows the results for the spin-triplet potential with $k_{1_0}=1.2\ k_F$, they are qualitatively unchanged both when $k_{1_0}=1.6\ k_F$ or $2.0\ k_F$ and when the spin-singlet potential is used. When $s_0\geq 2.0\ k_F$ the scattering amplitudes are closely approximated by their isolated-pair values.

A synopsis of the results for the spin-singlet potential specified by Eq. (14) and Table I, would be qualitatively the same as the one given above for the spin-triplet potential. Two quantitative differences appear: the scattering amplitude associated with the spin-singlet potential does not exhibit a bound-state pole either without or with the exclusion principle, and its

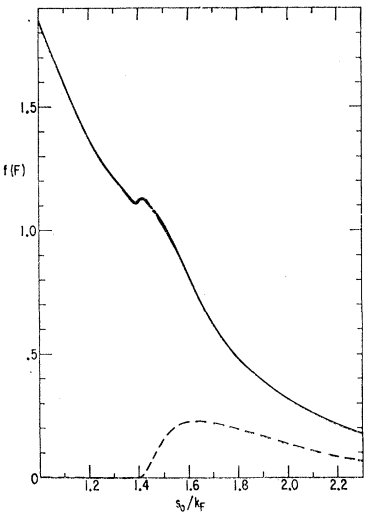

FIG. 13. Real and imaginary parts of an independent-pair scattering amplitude calculated for the Wheeler-Yamaguchi (Refs. 7, 8) potential with the parameters $\lambda=0.425$ F^{-3}, $\beta=1.46$ F^{-1}, and $k_F=1.42$ F^{-1}. The calculations were performed using Eqs. (8), (15), and (16) in the text. The solid and dashed lines represent the real and imaginary parts, respectively, of the scattering amplitude obtained for $(k_{1_0}/k_F)=1.2$ and $(k_{2_0}/k_F)=0.0$.

magnitude (in particular the magnitude of its imaginary part) is usually substantially reduced from the corresponding value obtained with the spin-triplet potential. The smaller value of β in the spin-singlet potential has the consequency that the spurious pole in the WY potential occurs at a larger value of k_0^2.

D. SUMMARY AND CONCLUSIONS

We have incorporated the influence of the exclusion principle on the two-body scattering problem by analyzing the BBG equation rather than the Schrödinger equation. For all values of the momentum of an interacting pair, both on and off the energy shell, the scattering amplitudes were evaluated for a separable interaction[7,8] which describes the low-energy nucleon-nucleon scattering data. In addition to poles corresponding to bound states of the interaction, the scattering amplitude exhibits poles resulting from the nonlocal nature of the interaction and, for certain two-body kinematics, Cooper poles. However, the poles resulting from the nonlocality of the interaction do not occur in the forward-scattering T matrices used in discussing the dispersion effect in low-density systems of interacting fermions. In the absence of single-particle potentials, numerical calculations of the scattering amplitudes lead to the following conclusions.

(a) For the spin-triplet nucleon-nucleon potential (which possesses a bound state), the independent-pair scattering amplitude is not well approximated by the isolated-pair scattering amplitude for Fermi-gas densities above the observed nuclear density divided by 512. This result is valid despite the fact that for the Fermi-gas density equal to the observed density divided by 512 we find that $(k_F/\beta)^3=0.002\ll 1$.

(b) For a repulsive potential with the same strength and range as the nucleon-nucleon spin-triplet potential the real part of independent-pair scattering amplitude is approximated to within 20% by the isolated-pair scattering amplitude for Fermi-gas densities less than one-eighth the observed nuclear density. For these densities $(k_F/\beta)^3\leq 0.115$. However, if the incident fermion has a wave vector which terminates close to the Fermi sphere, the imaginary part of the independent-pair scattering amplitude is only half as large as its isolated-pair counterpart at all densities above the observed nuclear density divided by 512.

(c) For potentials without bound states, the exclusion principle depresses the magnitude of both the real and the imaginary part of the scattering amplitude from their isolated-pair values.

(d) For potentials with bound states, the exclusion principle suppresses the bound-state pole in the scattering amplitude for sufficiently high Fermi-gas densities $[k_F\gtrsim 0.25\ (k_F)_{\text{obs}}]$ and $(\Lambda_0/2)\lesssim k_F$. Both the real and imaginary parts of the scattering amplitude associated with a pair of fermions can be considerably enhanced over their isolated-pair values when the Fermi-gas density is sufficiently high to move the bound-state pole in the scattering amplitude near zero relative energy of the pair.

ACKNOWLEDGMENTS

The author wishes to thank Professor J. A. Wheeler, Professor E. P. Wigner, and Dr. F. B. Malik for numerous stimulating discussions. The use of the GE 225 computer in the Information Studies Section of the General Electric Research Laboratory is gratefully acknowledged. Figures 5–8 were drawn by K. Staley.

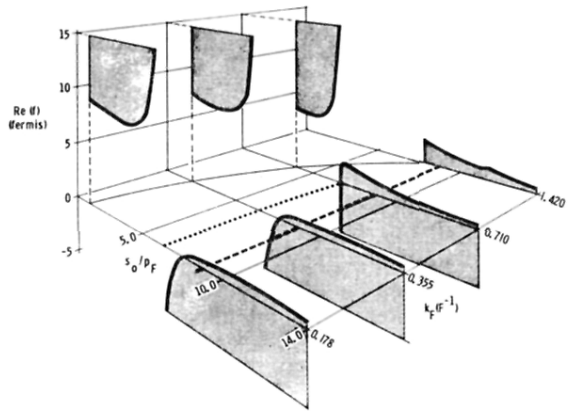

FIG. 5. The real part of the independent-pair scattering amplitude calculated for the Wheeler-Yamaguchi potential (Refs. 7, 8) with the parameters $\lambda=0.425$ F^{-3} and $\beta=1.46$ F^{-1}. The calculations were performed using Eqs. (8), (15), and (16) in the text with the kinematical parameters $k_{10}=1.562$ F^{-1}, $k_{20}=0.1775$ F^{-1}, and $\cos\theta=1.0$. The solid lines represent the real part of the scattering amplitude. The shading is included only for ease in visualization. The heavy dashed line indicates the energy-shell value, k_{10}, of s_0. The dotted line designates the location of the bound-state pole in the scattering amplitude. The curving light line at which the graphs of Re(f) begin indicates the point $s_0=k_F$ for the various values of k_F. The s_0 scale is measured in units of $p_F=(k_F)_{\text{obs}}/8$.

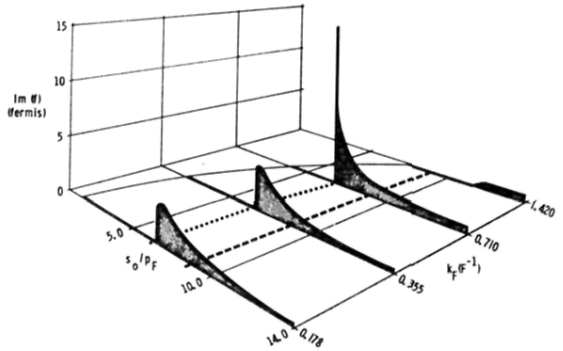

FIG. 6. The imaginary part of the independent-pair scattering amplitude calculated for the Wheeler-Yamaguchi (Refs. 7, 8) potential with the parameters $\lambda=0.425\ F^{-3}$ and $\beta=1.46\ F^{-1}$. The calculations were performed using Eq. (8), (15), and (16) in the text with the kinematical parameters $k_{1_0}=1.562\ F^{-1}$, $k_{2_0}=0.1775\,F^{-1}$, and $\cos\theta=1.0$. The solid lines represent the imaginary part of the scattering amplitude. The shading is included only for ease in visualization. The heavy dashed line indicates the energy-shell value, k_{1_0}, of s_0. The dotted line designates the location of the bound-state pole in the scattering amplitude. The curving light line at which the graphs of $\mathrm{Im}(f)$ begin indicates the point $s_0=k_F$ for the various values of k_F. The s_0 scale is measured in units of $p_F=(k_F)_{\mathrm{obs}}/8$.

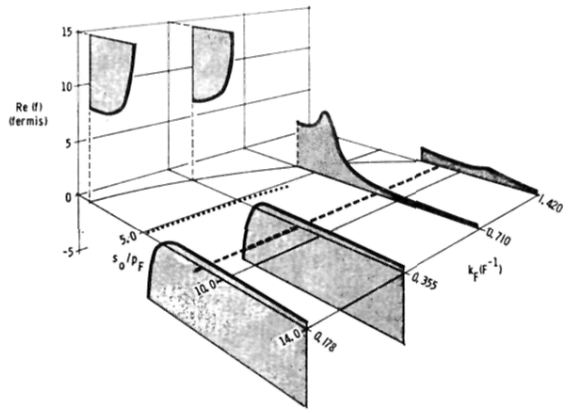

FIG. 7. The real part of the independent-pair scattinerg amplitude calculated for the Wheeler-Yamaguchi (Refs. 7, 8) potential with the parameters $\lambda=0.425$ F^{-3} and $\beta=1.46$ F^{-1}. The calculations were performed using Eqs. (8), (15), and (16) in the text with the kinematical parameters $k_{1_0}=1.562$ F^{-1}, $k_{2_0}=0.1775$ F^{-1}, and $\cos\theta=-1.0$. The solid lines represent the real part of the scattering amplitude. The shading is included only for ease in visualization. The heavy dashed line indicates the energy-shell value, k_{1_0}, of s_0. The dotted line designates the location of the bound-state pole in the scattering amplitude. The curving light line at which the graphs of Re(f) begin indicates the point $s_0=k_F$ for the various values of k_F. The s_0 scale is measured in units of $p_F=(k_F)_{\text{obs}}/8$.

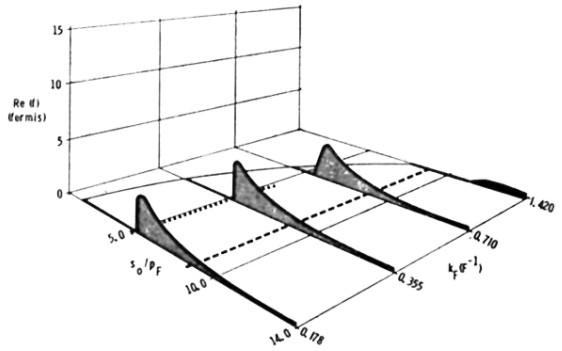

FIG. 8. The imaginary part of the independent-pair scattering amplitude calculated for the Wheeler-Yamaguchi (Refs. 7, 8) potential with the parameters $\lambda = 0.425 F^{-3}$ and $\beta = 1.46\ F^{-1}$. The calculations were performed using Eqs. (8), (15), and (16) in the text with the kinematical parameters $k_{1_0} = 1.562\ F^{-1}$, $k_{2_0} = 0.1775\ F^{-1}$, and $\cos\theta = -1.0$. The solid lines represent the imaginary part of the scattering amplitude. The shading is included only for ease in visualization. The heavy dashed line indicates the energy-shell value, k_{1_0}, of s_0. The dotted line designates the location of the bound-state pole in the scattering amplitude. The curving light line at which the graphs of $\mathrm{Im}(f)$ begin indicates the point $s_0 = k_F$ for the various values of k_F. The s_0 scale is measured in units of $p_F = (k_F)_{\mathrm{obs}}/8$.